Philosophical Magazine

ISSN: 1478-6435 (Print) 1478-6443 (Online) Journal homepage: https://www.tandfonline.com/loi/tphm20

Microalloying and the mechanical properties of amorphous solids

H. George E. Hentschel, Michael Moshe, Itamar Procaccia & Konrad Samwer

To cite this article: H. George E. Hentschel, Michael Moshe, Itamar Procaccia & Konrad Samwer (2016) Microalloying and the mechanical properties of amorphous solids, Philosophical Magazine, 96:14, 1399-1419, DOI: 10.1080/14786435.2016.1163433

To link to this article: https://doi.org/10.1080/14786435.2016.1163433

PHILOSOPHICAL MAGAZINE, 2016
VOL. 96, NO. 14, 1399–1419
http://dx.doi.org/10.1080/14786435.2016.1163433

Taylor & Francis
Taylor & Francis Group

Microalloying and the mechanical properties of amorphous solids

H. George E. Hentschel[a,b], Michael Moshe[c,d], Itamar Procaccia[a] and Konrad Samwer[e]

[a]Department of Chemical Physics, The Weizmann Institute of Science, Rehovot, Israel; [b]Department of Physics, Emory University, Atlanta, GA, USA; [c]Department of Physics, Syracuse University, Syracuse, NY, USA; [d]Department of Physics, Harvard University, Cambridge, MA, USA; [e]I. Physikalisches Institut, Universität Göttingen, Göttingen, Germany

ABSTRACT

The mechanical properties of amorphous solids like metallic glasses can be dramatically changed by adding small concentrations (as low as 0.1%) of foreign elements. The glass-forming-ability, the ductility, the yield stress and the elastic moduli can all be greatly effected. This paper presents theoretical considerations with the aim of explaining the magnitude of these changes in light of the small concentrations involved. The theory is built around the experimental evidence that the microalloying elements organise around them a neighbourhood that differs from both the crystalline and the glassy phases of the material in the absence of the additional elements. These regions act as *isotropic* defects that in unstressed systems modify the shear moduli. When strained, these defects interact with the incipient plastic responses which are quadrupolar in nature. It will be shown that this interaction interferes with the creation of system-spanning shear bands and increases the yield strain. We offer experimentally testable estimates of the lengths of nano-shear bands in the presence of the additional elements.

ARTICLE HISTORY
Received 26 February 2016
Accepted 3 March 2016

KEYWORDS
Plasticity; amorphous solids; defects; geometry

1. Introduction

The history of the production of amorphous metallic glasses spans by now more than seven decades. Originally, Buckel and Hilsch [1] accidentally formed amorphous metals by vapour deposition of one or several component systems onto an ultra-cold substrate. Later, Duwez [2] discovered that an alloy in its eutectic composition with an eutectic temperature as low as possible (Au–Si) is very much favoured to exist even at room temperature and above in a non-crystalline form. But only the intentional addition of a third or more element made *bulk* metallic glasses possible, for example A. Inoue's and W.L. Johnson's alloys in the early 1990s [3,4].

For more than 20 years it has been known that small additions of a further alloy component can greatly enhance the glass-forming-ability of metallic glasses, measured as the largest radius of a cylinder of a metallic glass without a crystalline core. In the last 10 years hundreds of microalloyed systems have been presented by the various active groups in China, US, Japan, Korea and Europe [5]. It was argued that an important effect

CONTACT Michael Moshe mmoshe@syr.edu; Itamar Procaccia itamar.procaccia@gmail.com

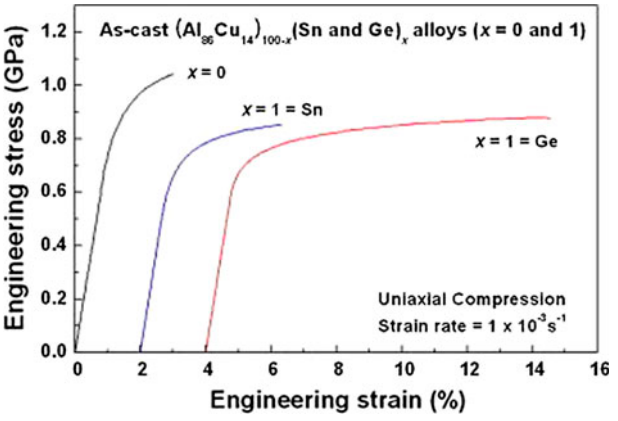

Figure 1. (colour online) The effect of a small concentration of an Sn and Ge on the toughness of Al–Cu metallic glass [27].

of adding a minute amount of foreign atoms is on the eutectic temperature of the mixture. There is a dip in the crystallisation temperature for a liquid system cooled down into the glass regime as a function of the microalloying concentration that reaches a minimum at some finite but small concentration (say 1%). Remarkable cusps have been observed in the glass-forming-ability of many alloys with a width in composition down to 0.1% or even less [5,6]. These cusps reflect exactly the extremely deep lying (in temperature) eutectic points. In other words, the liquid is extremely stabilised against partitioning into the stable crystalline or polycrystalline phases. Whether this is due to chemical or topological barriers is an actual debate. But this stabilisation of the liquid state down to extremely low temperatures by minute additions of another component can also be seen in the liquid properties like diffusion constants [7], formation of special local structures [8] or fragility [9]. Microalloying also delays the failure of metallic glasses, increasing its toughness as defined by the integral under the stress vs. strain curve, see Figure 1.

A number of papers in the literature have proposed that the short- and medium-range order in metallic glasses can be partially accounted for by icosahedra or quasi-crystalline clusters. Of course, such quasicrystalline clusters of atoms cannot grow beyond a certain size because of local frustration. This suggestion was originally proposed by Kivelson et al. [10]; this idea was extended by de Gennes [11]. For example, the atomic structure of the $Cu_{35}Zr_{65}$, $Cu_{50}Zr_{50}$ and $Cu_{65}Zr_{35}$ metallic glasses were investigated by means of high-energy X-ray diffraction and neutron diffraction, and the geometric short-range order found could be characterised by a variety of polyhedra [12]. Another example is the formation of an icosahedral quasicrystalline phase followed by crystallisation of tetragonal $CuZr_2$ which has been observed in the $Zr_{70}Cu_{29}Pd_1$ glassy alloy during annealing up to 850 K [13].

Molecular dynamics simulations have given similar clues. For example, Lekka et al. [14] concluded from molecular dynamic simulations of $Cu_{46}Zr_{54}$ glasses that 23% of the atoms belonged to Cu– centred icosahedral clusters and about 41% belonged to Zr– centred clusters. While Lee et al. [15] showed that in molecular dynamics simulations of a $Cu_{65}Zr_{35}$ there were polyhedral clusters, of which 15% were ideal icosahedra.

Perhaps the most likely clusters formed in metallic glasses are the Frank–Kasper [16] close-packed clusters whose quasicrystalline short-range order is incompatible with either

the ground state crystalline symmetry of the surrounding matrix or the random metallic glass phase. In some cases [8] these form as much as 20% of the observed clusters. Thus in NiP glasses up to 16% of such Kasper polyhedra have been found, while in $Ni_{81}B_{19}$ metallic glasses Kasper polyhedra are dominant (at about 17.8 and 7.1%, respectively). In fact, it has been proposed that Kasper polyhedral short-range order is the main underlying topological short-range order in metallic glasses.

In this paper, we propose that the microalloying particles may be nucleating a patch of a new local structure around themselves that frustrates the formation of the pure crystalline phase, being incompatible with both the equilibrium crystalline order and with the glassy disorder. Whether these patches are crystalline (with different crystal structure than the thermodynamic equilibrium phase of the unadulterated glass) or icosahedral (quasicrystalline) in nature is still debated but will not be important for our considerations.

Accepting the point of view that the microalloying particles organise around them a local structure that differs from the bulk structure, we will treat them in this paper as *defects* in the bulk structure, and seek a theoretical explanation for their influence on the mechanical properties of the glass. Importantly, we will assert that on scales larger than the local patches around the foreign elements these defects interact isotropically (i.e. the defects have spherical symmetry). We will show that they interact with the plastic events that occur in metallic glasses under straining, and the latter are *not* spherically symmetric. Rather, plastic events have quadrupolar symmetry as predicted by the theory of Eshelby inclusions [17], and see also [18]. In two dimensions the difference is easy to characterise, in terms of the SO(2) symmetry group; we treat the isotropic defect as having an $\ell = 0$ characteristic whereas the plastic quadrupolar displacement fields associated with plastic instabilities have an $\ell = 2$ characteristic.

In Section 2, we review the theory of the mechanical instability in amorphous solids that leads to shear banding, and explain why the existence of even a *single* isotropic defect can defer the instability, leading to higher toughness of the material. For the sake of clarity and simplicity, we limit the discussion to systems in two dimensions. The generalisation to three dimensions will be commented upon in the last section. In Section 3 we treat a density of $\ell = 0$ defects and show that it is expected to result in increasing the toughness of the material, leading to the appearance of arrested shear bands of finite length. The expected length of the arrested shear bands is estimated in Section 4. We also explain why an even larger concentration of foreign elements is *not* beneficial for increasing the toughness of the material. These predictions should be tested in experiments. Finally, Section 5 offers a summary, a discussion and some comments about the road ahead.

2. The effect of a single isotropic defect on the shear banding instability in two dimensions

In this section, we construct the theoretical framework to discuss the effect of isotropic ($\ell = 0$) defects on the shear banding instability in two-dimensional amorphous solids. We begin with a short review of the microscopic theory of the shear banding instability in the unadulterated glass.

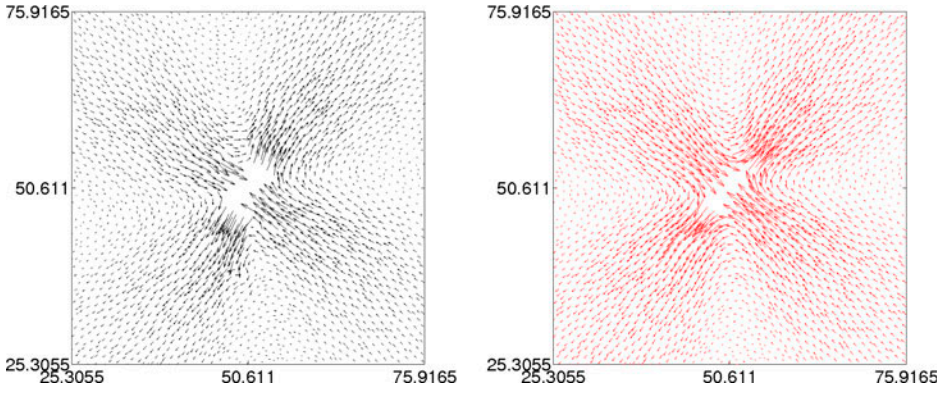

Figure 2. (colour online) A window into the simulations cell with coordinates in Lennard-Jones units. Notes: Shown is a typical plastic instability at small values of the external strain. Left panel: the displacement field associated with the plastic event as observed in numerical simulations, cf. Ref. [21]. Right panel: the displacement field of an Eshelby solution where the eigenstrain and the core-size were fitted to the numerically found instability. The quadrupolar structure with power law decay towards infinity is obvious.

2.1. Review of the shear banding instability in two-dimensions

Plastic responses in amorphous solids are sensitive to temperature effects, strain rates and the mode of external loading. For simplicity and concreteness in the present discussion we will focus on amorphous solids in athermal conditions ($T = 0$ or in practice $T \ll T_g$ where T_g is the glass transition temperature). We will also limit ourselves to pure external shear strains which are area preserving since the nature of the shear banding instability is sensitive to loading that is non-area preserving, cf. [22]. Denoting the external strain by γ (without tensorial indices since we have only shear strain), we consider the limit $\dot{\gamma} \to 0$ (quasi-static conditions) where the theory appears in its cleanest form. The numerical protocol used to produce the results shown below in Figures 2 and 3 is described in Appendix 1. Under these conditions, plastic instabilities are identified by the vanishing of an eigenvalue of the Hessian matrix of the system. Denoting the total energy of the system by $U(\boldsymbol{r}_1, \boldsymbol{r}_2, \ldots \boldsymbol{r}_N)$ where $\{\boldsymbol{r}_i\}_{i=1}^N$ is the array of particle positions, the Hessian matrix is defined by

$$H_{i,j} \equiv \frac{\partial^2 U(\boldsymbol{r}_1, \boldsymbol{r}_2, \ldots \boldsymbol{r}_N)}{\partial \boldsymbol{r}_i \partial \boldsymbol{r}_j} \tag{1}$$

As long as all the eigenvalues of the (symmetric and real) Hessian matrix $\boldsymbol{H}$ are positive, the system is stable. Plasticity is the consequence of an instability with at least one of the eigenvalues λ_p going to zero at some value of the strain $\gamma = \gamma_P$. It was shown that at that value of the strain the associated eigenfunction Ψ_p localises on the particles that participate in the plastic events [19]. In fact the eigenfunction which is extended as long as $\lambda_p > 0$ localises precisely on the non-affine plastic displacement field that is associated with the plastic instability.

The nature of the displacement field associated with the plastic instability differs dramatically when γ is small and when γ is large. For small values of γ, when the system is deep in the 'elastic' region, plastic events are small (localised), having a quadrupolar structure that is excellently modelled by the displacement field associated with an Eshelby inclusion, cf.

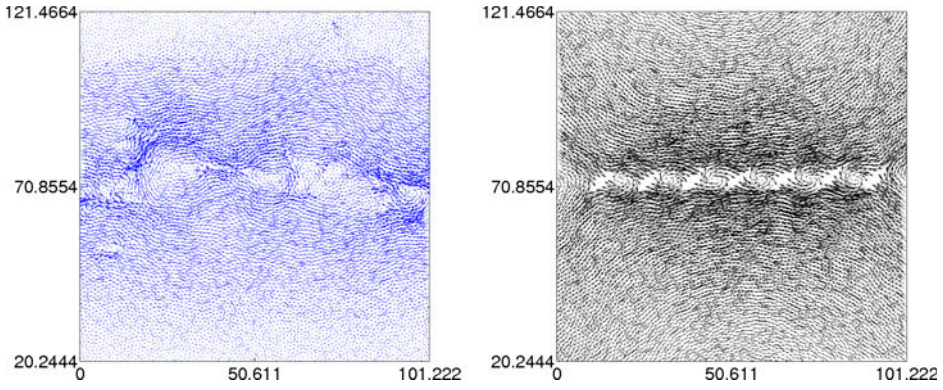

Figure 3. (colour online) A window into the simulations cell with coordinates in Lennard-Jones units. Notes: Typical plastic instability at large values of the external stain. Left pannel: the displacement field associated with a system-spanning plastic event, localizing the displacement around a narrow line [21]. Right panel: a model of the same event using a series of Eshelby quadrupoles. Now there exists a global connection between the outgoing and ingoing displacement fields on the quadrupoles, localising the displacement on a thin line.

Figure 2. At larger values of γ, above some theoretically computable value γ_Y, the instability appears as the simultaneous inception of a whole line of quadrupoles, system spanning, which organise the displacement field on a narrow line with the displacement field pointing in opposite directions above and below the line, see Figure 3. It was shown [20,21] that the single quadrupole solution is a minimal energy solution as long as $\gamma < \gamma_Y$ but when $\gamma > \gamma_Y$ the system-spanning line of quadrupoles is winning, being the minimal energy solution. This solution requires that the quadrupoles will be 'in phase', meaning that the stable (respectively unstable) direction of every quadrupole is parallel to the stable (respectively unstable) direction of every other quadrupole. In other words, the quadrupoles are oriented in the same way with respect to the line joining their cores, and this line should be at 45° with respect to the principal stress axis. The reader is referred to Refs. [20–22] for a full explanation of these findings. In the next subsection, while preparing for the analysis of the effect of the $\ell = 0$ defect, we will shed more light on the phenomenon. It is important to stress that in the quasi-static strain controlled protocols which are used in our numerical simulations the 'strain rate' is always zero, even when system spanning plastic instabilities take place. One is increasing the strain infinitesimally and the system is allowed to complete its non-affine response before the strain is increased further.

2.2. Theoretical considerations

The elastic energy of interaction between $\ell = 0$ and $\ell = 2$ defects can be modelled as the interaction between Eshelby inclusions, where the case of $\ell = 2$ corresponds to a purely deviatoric inclusion, and the case of $\ell = 0$ corresponds to a purely isotropic inclusion. A calculation for the interaction between two $\ell = 2$ defects was presented in [20,21]. Although it is possible to extend the calculations shown in [20,21] to include both $\ell = 0$ and $\ell = 2$ defects, here we adopt a different approach whose elaboration can be found in Refs. [23,24]. This approach relies on a geometric formulation of incompatible elasticity. According to this approach, localised plastic deformations are sources for residual stresses,

Table 1. Elastic charge sources $\bar{K}$ and their corresponding elastic potentials ψ. The superscript 'T' refers to 'transpose'.

Type	$\bar{K}$	ψ
Point	$\frac{1}{2}P\,\Delta\delta(\mathbf{x})$	$(YP/4\pi)\ln\lvert\mathbf{x}\rvert$
Quadrupole	$\frac{1}{4}(\nabla^T\cdot\mathbf{Q}\cdot\nabla)\delta(\mathbf{x})$	$(Y/16\pi)\,(\hat{\mathbf{x}}^T\cdot\mathbf{Q}\cdot\hat{\mathbf{x}})$
External stress	–	$\frac{1}{2}(\mathbf{x}^T\cdot\mathrm{Cof}(\sigma)\cdot\mathbf{x})$

whose energetic implications are very similar to those of charge densities in electrostatics. These stress densities are quantified by a single scalar function $\bar{K}$, and in the case of an elastic solid they act as source terms for the Airy stress function ψ which solves the bi-Laplace equation

$$\Delta\Delta\psi(\mathbf{x}) = Y\bar{K}(\mathbf{x}), \tag{2}$$

where Δ is the Laplace operator and Y is the Young's modulus.

For example, the far field description of an $\ell = 0$ defect within this formulation is given by an elastic charge singularity of the form

$$\bar{K}(\mathbf{x}) = \frac{1}{2}P\Delta\delta(\mathbf{x}). \tag{3}$$

Here $P = \pi a_{\mathrm{iso}}^2\epsilon_{\mathrm{iso}}^*$ where a_{iso} will take the physical meaning the core size of the isotropic 'patch' around our microalloying particle and $\epsilon_{\mathrm{iso}}^*$ is the eigengstrain associated with the isotropic inclusion. Positive or negative values of P correspond, respectively, to expansion or contraction due to the inclusion.

In electrostatics, two singular charge densities ρ_1 and ρ_2 induce electrostatic potentials ϕ_1 and ϕ_2 through the Poisson's equation. The interaction between two such electric charge densities is $U_{el} = \int \phi_1(\mathbf{x})\rho_2(\mathbf{x})\,\mathrm{d}\mathbf{x}$. In [24], it was shown that the same holds for elastic stress densities. That is, consider two singular stress densities described by $\bar{K}_1$ and $\bar{K}_2$. Each of these induces (through Equation (2)) an elastic potential denoted as ψ_1 and ψ_2. The energy associated with their interaction is

$$U = \int \psi_1(\mathbf{x})\bar{K}_2(\mathbf{x})\,\mathrm{d}\mathbf{x} = \int \psi_2(\mathbf{x})\bar{K}_1(\mathbf{x})\,\mathrm{d}\mathbf{x}. \tag{4}$$

This result is the key for obtaining simple explicit expressions for the interactions between defects, and their interactions with external fields.

A short list of possible singularities $\bar{K}$ together with their corresponding elastic potentials ψ are listed in Table 1.

Here ∇ is the nabla operator, $\mathbf{Q}$ is a traceless symmetric matrix

$$\mathbf{Q} = \begin{pmatrix} Q_1 & Q_2 \\ Q_2 & -Q_1 \end{pmatrix}, \tag{5}$$

and Cof(·) is the Cofactor of the matrix concerned.

Given a purely deviatoric inclusion oriented with angle θ measured from the x axis, its quadrupolar charge is

$$\mathbf{Q} = Q \begin{pmatrix} \cos 2\theta & \sin 2\theta \\ \sin 2\theta & -\cos 2\theta \end{pmatrix}. \tag{6}$$

Here $Q = \pi a_{\text{quad}}^2 \epsilon_{\text{quad}}^*$ with, as before a_{quad} being the core size of the quadrupolar singularity and ϵ_{quad}^* its eigenstrain. Given *two* such deviatoric inclusions with magnitudes Q_1 and Q_2, oriented by θ_1 and θ_2 measured from the line connecting them, their elastic interaction energy is obtained by substituting ψ of one quadrupole and $\bar{K}$ of the second quadrupole in Equation (4):

$$U_{QQ} = \frac{YQ_1Q_2}{16\pi r^2} \cos(2\theta_1 + 2\theta_2). \tag{7}$$

Similarly, we obtain an expression for the interaction between an $\ell = 0$ defect located at the origin, with an $\ell = 2$ defect located at distance r, with an orientation θ measured from their connecting line

$$U_{QP} = \frac{YQP}{8\pi r^2} \cos(2\theta). \tag{8}$$

With an external fields present, its interaction with the quadrupoles should be taken into account. Using the same procedure (see for e.g. [23]), we find that the interaction of an external shear σ with a quadrupole is

$$U_{Q\gamma} = -\frac{1}{2} QY\gamma \sin(2\theta) \tag{9}$$

where now θ is measured from the direction of the shear's principal axis, taken below to be the x axis. Here γ is the strain measured with respect to an appropriate reference point. Note that external fields do *not* interact with $\ell = 0$ defects.

2.3. Formation of shear band without microalloying

In previous work, it was shown that when the external strain is sufficiently large, a line of quadrupoles cab appear spontaneously as a result of plastic instability. Their orientations appear highly correlated. To see this using the present formalism deduce from Equation (9) that the energy is minimised for $\theta = \pi/4$ (for positive strain).

To explain the formation of the quadrupoles along a line, we examine their interaction with each other, rewriting Equation (7) for a general orientation of the line with respect to the x axis:

$$U_{\text{QQ}} = \frac{YQ^2}{16\pi r^2} \cos(2\theta_1 + 2\theta_2 - 4\phi), \tag{10}$$

where ϕ is the angle between the x axis and the line that connects the quadrupoles. This interaction energy is minimised for $2\theta_1 + 2\theta_2 - 4\phi = \pi$. In the absence of an external field there is a degeneracy in the energy minimising configurations. Two representative energy minimising configurations are shown in Figure 4. When an external shear exists, the energy is minimised for $\phi = 0$, that is the quadrupoles are aligned parallel to the external shear, all with the same angle of $\pi/4$. These results hold for any set of quadrupoles; given N quadrupoles subjected to external shear, their optimal position is along a line with the

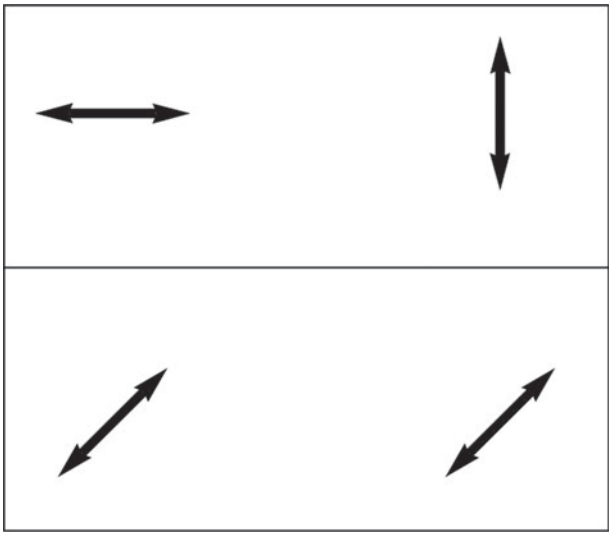

Figure 4. Possible relative orientations of two quadrupoles that minimise their interaction energy without an external strain. With external shear strain the degeneracy is removed, and only the lower panel survives.

same orientation of $\pi/4$. Arranged like this they form a connection between the incoming and outgoing directions of the quadrupolar displacement field, resulting in a shear band. It was shown in Refs. [20,21] that at sufficiently large external strain $\gamma \geq \gamma_{\rm Y}$ this solution is energetically favourable compared to a single localised quadrupolar displacement field. We will explain now that in the presence of isotropic defects one must increase γ further to allow for the spontaneous appearance of this system-spanning instability.

2.4. The effect of an isotropic defect

An $\ell = 0$ defect describes the uniform expansion or contraction of a small region inside a material. We rewrite now Equation (8) for a general orientation

$$U_{\rm QP} = \frac{YPQ}{8\pi r^2} \cos\left(2\theta - 2\phi\right), \tag{11}$$

where the isotropic defect is at the origin and the quadrupole is at a point (r, ϕ). The angle θ is the quadrupole orientation.

Now the value of θ that minimises the energy depends on the sign of P. In Figure 5, we show two different optimal relative configurations of the quadrupole associated with opposite signs of P. One should note that it is *not* the size of the microalloying atom which is at stake here, but rather the contraction or expansion effect of the organised patch around the atom. Much work had been devoted to analyzing 'small' or 'large' atoms [25], but in reality the important physics lies in their ability to nucleate patches rather than their own size. In these notes we assume a contraction ($P < 0$), hence the minimiser is obtained for

$$\theta + \phi = \pi/2, \tag{12}$$

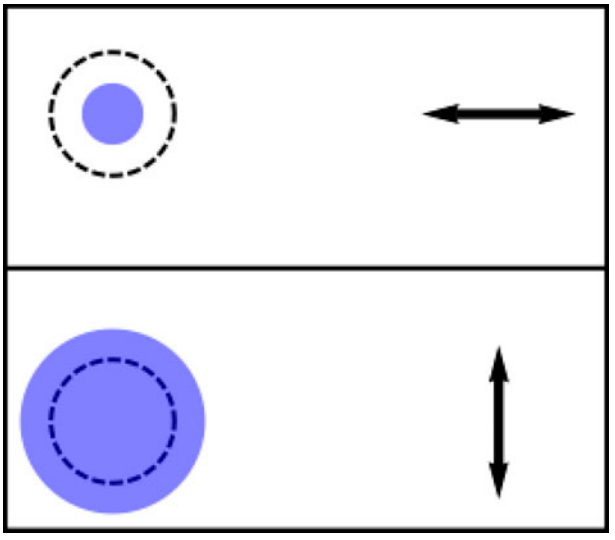

Figure 5. (colour online) The orientations of a quadrupole that minimise its interaction energy with an $\ell = 0$ defect. The two orientations are associated with a negative or a positive P.

meaning that the quadrupole is perpendicular to the connecting line of the quadrupole and the isotropic defect.

2.5. Array of quadrupoles near a single isotropic defect

In this subsection, which is central to our theory, we demonstrate how the existence of a single isotropic defect interfere with the creation of a shear band via a system spanning plastic instability.

Consider a linear array of $2N$ quadrupoles with charges Q, positioned at $(x_i, y_i) = ((2i+1)L, r)$, having orientations θ_i, with $i \in (-N, -N+1, \ldots, N-2, N-1)$. At the origin there is an isotropic defect of strength P, and the system is subjected to external strain. The elastic interaction energy is

$$\begin{aligned} U &= -\frac{1}{2}Y\gamma Q\sum_i \sin(2\theta_i) + \sum_{i\neq j}\frac{EQ^2}{16\pi r_{ij}^2}\cos(2\theta_i + 2\theta_j) \\ &\quad + \frac{YPQ}{8\pi}\sum_i\left(\frac{x_i^2 - y_i^2}{(x_i^2+y_i^2)^2}\cos(2\theta_i) + \frac{2x_iy_i}{(x_i^2+y_i^2)^2}\sin(2\theta_i)\right) \\ &\quad + U_S. \end{aligned} \tag{13}$$

where $\boldsymbol{r}_{ij}$ are the vector distances between the quadrupoles i and j and U_S is composed of the self energies of the quadrupoles and the isotropic defect.

At this point, we seek the orientation of the set of quadrupoles that minimises the total elastic energy. For $P = 0$ the problem is reduced back to the one studied in [20,21]. The result in this case is simply $\theta_i = \pi/4$.

In the presence of an isotropic defect, the problem cannot be solved analytically, and we resort to a numerical solution. There are three independent dimensionless parameters in Equation (13). The first is the ratio of amplitudes of the isotropic and quadrupolar defect

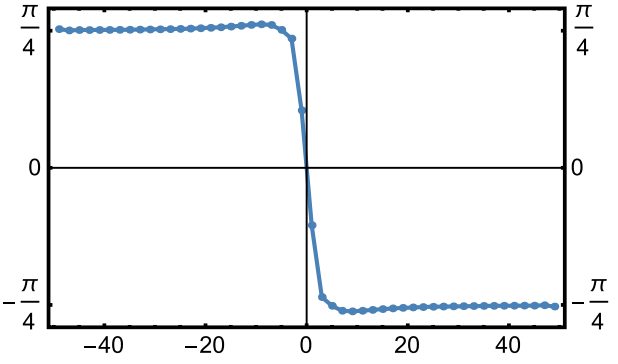

Figure 6. (colour online) The angle of the quadrupole θ of the set of 50 quadrupoles in the presence of an isotropic defect $\hat{p} = 5, \zeta = 5$, and no shear $\Gamma = 0$.

$\hat{p} = P/Q$. The second is the scaled distance $\zeta = r/L$ and last is the rescaled external strain $\Gamma = \gamma \frac{L^2}{Q}$. In the following figures, we plot the optimal orientations of quadrupoles for several values of $\hat{p}, \zeta, \Gamma$. In Figure 6 we show the optimal orientation of a set of 50 quadrupoles in the presence of an isotropic defect with $\hat{p} = 5$, $\zeta = 5$, and no external strain, i.e. $\Gamma = 0$.

The x axis in this figure corresponds to the position of the quadrupole along the line, and the y axis corresponds to the angle θ of the direction of the quadrupole that minimised the elastic energy. Note that when there is no external strain, there are two equal orientations $\theta = \pm\pi/4$ for which the energy of the line of quadrupoles is at a minimum. When an istorpic defect is placed at the origin, this can cause a flip from $\theta = \pi/4$ to $\theta = -\pi/4$. We should stress however that at $\gamma = 0$ one does not expect a line of quadrupoles, since the single quadrupole solution has a lower energy.

In Figure 7 we plot a similar graph, for several non-zero external shear strains $\Gamma = (5 \times 10^{-3}, 10^{-2}, 3 \times 10^{-2}, 10^{-1}, 3 \times 10^{-1})$. With a finite external strain the preferred angle θ sufficiently far from the $\ell = 0$ defect is always $\theta = \pi/4$. The presence of the defect perturbs this angle, with the quadrupoles that are closest to the defect being disturbed most. Note the asymmetry in the amount of perturbations of the angles of the quadrupoles on the right and on the left parts of the isotropic defect. This stems from the fact that the *positions* of the quadrupoles are right-left symmetric, their orientation is not. The interactions with quadrupoles on the right and on the left are not the same.

Of course, with the quadrupoles perturbed, the associated displacement field cannot be described by a thin system spanning shear-band. In order to obtain a spanning shear-banding instability one needs to increase the external strain to overcome the perturbation of the isotropic defect. While this does not provide yet a full explanation to the data shown in Figure 1, it indicates the physical origin of the phenomenon. To understand it fully we need to consider a density of isotropic defects as done in the next section.

For completeness, we show results of a similar calculation for a given value of the external strain but with other values of $\hat{p}$ and ζ. In Figure 8 we take $\zeta = 5$, $\Gamma = 0.1$, and $\hat{p} = (1, 3, 5, 10, 20)$. In Figure 9 we take $\hat{p} = 5$, $\Gamma = 0.1$, and $\zeta = (2, 4, 6, 10, 15)$.

The reader should note the interesting up-down-up oscillation in the response of the computed angles to the presence of the isotropic defect. The upward oscillation can be interpreted as a screening effect.

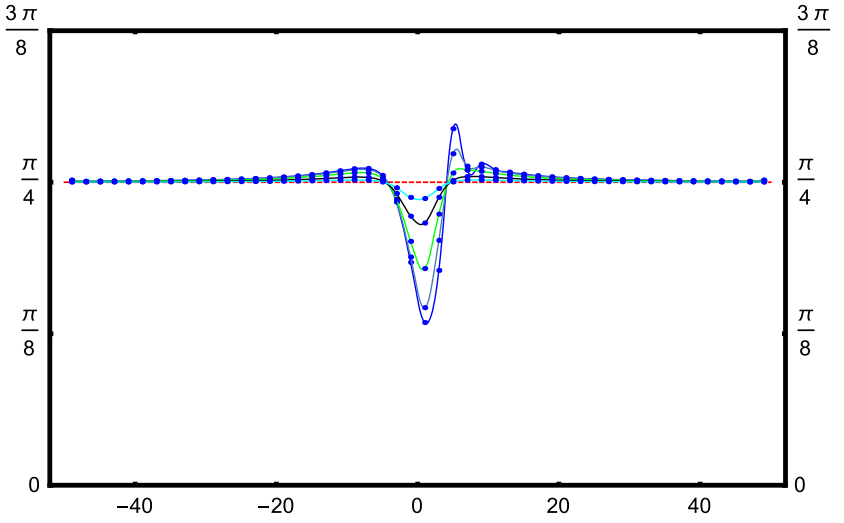

Figure 7. (colour online) The angle of the quadrupole θ of the set of 50 quadrupoles in the presence of an isotropic defect $\hat{p} = 5, \zeta = 5$, and for various shear values: $\Gamma = 5 \times 10^{-3}, 10^{-2}, 3 \times 10^{-2}, 10^{-1}, 3 \times 10^{-1}$). As the external strain is increased the effect of the perturbation decreases.

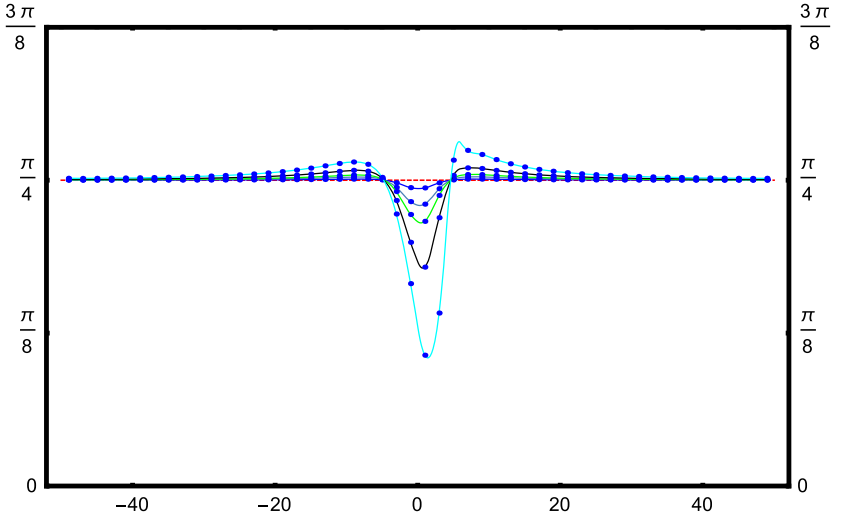

Figure 8. (colour online) The angle of the quadrupole θ of the set of 50 quadruoples in the presence of an isotropic defect $\Gamma = 0.1, \zeta = 5$, and for various values of $\hat{p}$: $\hat{p} = 1, 3, 5, 10, 20$. As $\hat{p}$ is increased the effect of the $\ell = 0$ defect strengthens.

3. The increase in yield strain due to a density of isotropic defects

In this section, we attempt to demonstrate the increase in the yield strain due to the existence of a density of $\ell = 0$ defects. To this aim we consider below an infinite two-dimensional body containing a dilute array of isotropic defects. As a preparatory step, we consider first a square array of isotropic defects of fixed strength P. Understanding this easier case will help later with the case of a random distribution of isotropic defects.

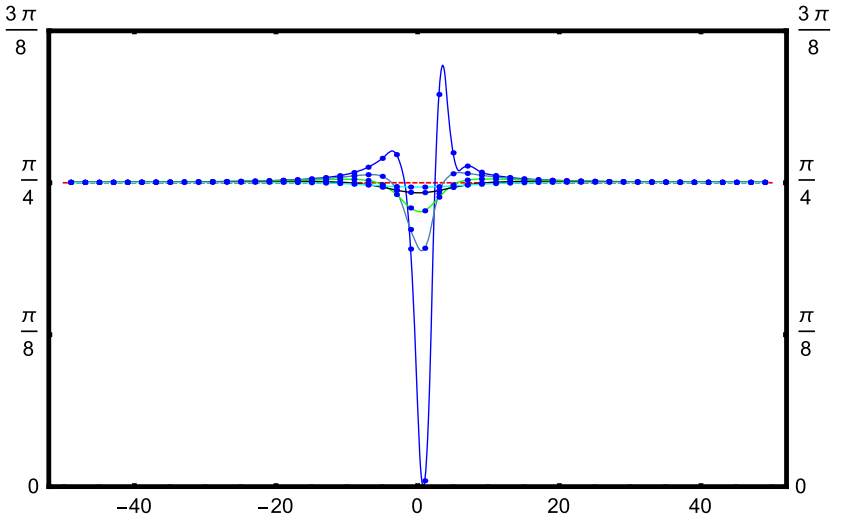

Figure 9. (colour online) The angle of the quadrupole θ of the set of 50 quadrupoles in the presence of an isotropic defect $\hat{p} = 5$, $\Gamma = 0.1$, and for various values of ζ: $\zeta = 2, 4, 6, 10, 15$. As ζ increases the effect of the $\ell = 0$ defect decreases.

Denote as l_p the distance between neighbouring isotropic defects. With $(i, j) \in \mathbb{N} \times \mathbb{N}$ their positions in cartesian coordinates are

$$(x_i, y_j) = ((\alpha + i) \cdot l_p, (\beta + j) \cdot l_p) \,, \quad 0 < \alpha, \beta < 1 \,. \tag{14}$$

The material is subjected to external shear strain γ, and the elastic energy stored in the system at this stage is set to zero. At this point, we ask if the formation of a linear array of quadrupoles can reduce the elastic energy stored in the system.

We start with a single quadrupole located at the origin. This quadrupole interact with the external shear and with the isotropic defects. In addition it contributes a self-interacting term to the elastic energy. The interaction energy of such quadrupole with an isotropic defect located at (x_0, y_0) is

$$E_{qp} = \frac{PQY}{2\pi} \left(\frac{x_0^2 - y_0^2}{\left(x_0^2 + y_0^2\right)^2} \cos 2\theta + \frac{2x_0 y_0}{\left(x_0^2 + y_0^2\right)^2} \sin 2\theta \right) \tag{15}$$

Substituting the positions of the isotropic defects and summing over all of them we find the elastic energy interaction

$$E_{qp}^i = \frac{PQY}{2\pi} \left(f(\alpha, \beta) \cos 2\theta_i + g(\alpha, \beta) \sin 2\theta_i \right) , \tag{16}$$

where

$$f(\alpha, \beta) = \frac{1}{l_p^2} \sum_{i=-\infty}^{\infty} \sum_{j=-\infty}^{\infty} \frac{x_i^2 - y_j^2}{\left(x_i^2 + y_j^2\right)^2} \equiv \frac{1}{l_p^2} \tilde{f}(\alpha, \beta), \tag{17}$$

and

$$g(\alpha,\beta)=\frac{1}{l_p^2}\sum_{i=-\infty}^{\infty}\sum_{j=-\infty}^{\infty}\frac{2x_iy_j}{\left(x_i^2+y_j^2\right)^2}\equiv\frac{1}{l_p^2}\tilde{g}(\alpha,\beta). \tag{18}$$

Note that for the case of a random distribution of defects f and g are different for each quadrupole, and therefore effectively α and β are functions of quadrupoles positions. We will use this later.

The interaction with the external shear is

$$E_{\text{Shear}}=-\frac{1}{2}YQ\gamma\sin 2\theta\,, \tag{19}$$

and the self interaction term is

$$E_{\text{Self}}=\frac{YQ^2}{16\pi a^2}\,. \tag{20}$$

Since we are interested in a linear array of quadrupoles, we consider a domain in the material $(x,y)\in[0,L]\times[-\infty,\infty]$, with a set of quadrupoles located at $(x_i,y_i)=(i\cdot l_q,0)$. Here l_q is the distance between the quadrupoles. We further simplify the problem by assuming $L=k\cdot l_q=n\cdot l_p$, that is the length L is equal to an integer multiple of l_p, and so is $l_q=m\cdot l_p$.

We denote by $\rho_p\equiv\frac{n}{L}=\frac{1}{l_p}$ the isotropic defects density, and $\rho_q\equiv\frac{k}{L}=\frac{1}{l_q}$ the quadrupoles density. In addition to the list of interactions mentioned above, each quadrupole interacts now with all the other quadrupoles. This interaction energy of the i'th quadrupole with all the others is

$$E_{qq}^{i}=\sum_{j\neq i}\frac{YQ^2}{16\pi R_{ij}^2}\cos\left(2\theta_i+2\theta_j\right) \tag{21}$$

Substituting the quadrupoles locations we find

$$E_{qq}^{i}=\frac{YQ^2}{16\pi l_q^2}\sum_{j=-\infty}^{\infty}\frac{\cos\left(2\theta_i+2\theta_j\right)}{(i-j)^2} \tag{22}$$

We will use now all the results above for the calculation of the slope of the energy per unit length, vs. quadrupoles density.

We have k quadrupoles in the considered domain. Therefore the elastic energy stored in the domain is

$$E_L=\sum_{i=1}^{k}E_{\text{Self}}+E_{pq}^{i}+E_{\text{Shear}}^{i}+E_{qq}^{i} \tag{23}$$

The total energy stored in the system is $E_{\rm tot} = \frac{L_\infty}{L} \cdot E_L$, where L_∞ is the size of the system which goes to infinity. The energy per unit length is therefore

$$\begin{aligned}\frac{E_{\rm tot}}{L_\infty} &= \frac{k}{L} \cdot \frac{YQ^2}{16\pi a^2} \\ &\quad + \frac{PQY}{2\pi L} \sum_{i=1}^{k} \left(f(\alpha,\beta) \cos 2\theta_i + g(\alpha,\beta) \sin 2\theta_i \right) \\ &\quad - \frac{YQ\gamma}{L} \frac{1}{L} \sum_{i=1}^{k} \sin 2\theta_i + \sum_{i=1}^{k} E^i_{qq}. \end{aligned} \tag{24}$$

Using the following abbreviation

$$\langle \dots \rangle = \frac{1}{k} \sum_{i=1}^{k} \tag{25}$$

the above equation reads

$$\begin{aligned}\frac{E_{\rm tot}}{L_\infty} &= \frac{k}{L} \cdot \frac{YQ^2}{16\pi a^2} \\ &\quad + \frac{PQY}{2\pi L} k \left(f(\alpha,\beta) \langle \cos 2\theta_i \rangle + g(\alpha,\beta) \langle \sin 2\theta_i \rangle \right) \\ &\quad - \frac{YQ\gamma k}{L} \langle \sin 2\theta_i \rangle + \frac{1}{L} \sum_{i=1}^{k} E^i_{qq}. \end{aligned} \tag{26}$$

The last term in this expression is

$$\begin{aligned}\frac{1}{L} \sum_{i=1}^{k} E^i_{qq} &= \frac{k}{L} \cdot \frac{YQ^2}{16\pi l_p^2} \left\langle \sum_{j=-\infty}^{\infty} \frac{\cos\left(2\theta_i + 2\theta_j\right)}{(i-j)^2} \right\rangle \\ &= \frac{YQ^2}{16\pi} \rho_q^3 \left\langle \sum_{j=-\infty}^{\infty} \frac{\cos\left(2\theta_i + 2\theta_j\right)}{(i-j)^2} \right\rangle \end{aligned} \tag{27}$$

Since this term scales like ρ_q^3 it does not contribute to the slope at $\rho_q = 0$. Therefore, the first three terms in $\frac{E_{\rm tot}}{L_\infty}$, which are linear in ρ_q, are the only relevant terms for this problem.

$$\begin{aligned}\left(\frac{\partial}{\partial \rho_q} \frac{E_{\rm tot}}{L_\infty} \right)_{\rho_q = 0} &= \frac{YQ^2}{16\pi a^2} \\ &\quad + \frac{PQY}{2\pi} \left(f(\alpha,\beta) \langle \cos 2\theta_i \rangle + g(\alpha,\beta) \langle \sin 2\theta_i \rangle \right) \\ &\quad - YQ\gamma \langle \sin 2\theta_i \rangle . \end{aligned} \tag{28}$$

Defining

$$\gamma_c \equiv \frac{Q}{16\pi a^2} \frac{1}{\langle \sin 2\theta \rangle} + f(\alpha,\beta) \frac{P}{2\pi} \frac{\langle \cos 2\theta \rangle}{\langle \sin 2\theta \rangle} + g(\alpha,\beta) \frac{P}{2\pi} \tag{29}$$

we get

$$\left(\frac{\partial}{\partial\rho_q}\frac{E_{\rm tot}}{L_\infty}\right)_{\rho_q=0} = \left(\frac{YQ^2}{16\pi a^2}+\frac{PQY}{2\pi}\Big(f(\alpha,\beta)\,\langle\cos 2\theta_i\rangle + g(\alpha,\beta)\,\langle\sin 2\theta_i\rangle\Big)\right)\times\left(1-\frac{\gamma}{\gamma_c}\right). \tag{30}$$

This is the main result of this section. We will now explain its implications for the problem at hand.

The defects magnitude P has the dimensions of squared length. We therefore define the dimensionless parameter $\eta=\frac{P}{l_p^2}$ as the dilution of the isotropic defects.

Start with the limit $\eta\to 0$ where there are no isotropic defects. This limit is achieved equivalently using $P\to 0$ or $l_p\to\infty$. In this limit

$$\gamma_c \equiv \frac{Q}{16\pi a^2}\frac{1}{\langle\sin 2\theta\rangle}. \tag{31}$$

In the absence of isotropic defects the energy is minimised for $\theta_i=\pi/4$, hence

$$\gamma_c \equiv \frac{Q}{16\pi a^2}, \tag{32}$$

which is consistent with the result of Ref. [21].

Next we consider the limit of small nonzero dilution $|\eta|\ll 1$. In this limit the energy minimising orientations θ_i deviate slightly from $\pi/4$. We find

$$\sin 2\theta_i \approx 1-\eta^2\delta_i^2\,, \tag{33}$$

$$\cos 2\theta_i \approx -\eta\delta_i\,. \tag{34}$$

Expanding γ_c in powers of η we find

$$\gamma_c=\gamma_c^0+\frac{\tilde{g}(\alpha,\beta)-2\tilde{f}(\alpha,\beta)\,\langle\delta_i\rangle}{2\pi}\eta+O(\eta^2) \tag{35}$$

This shows that the critical value of the external shear may increase or decrease. We now explain the relevance of these findings to the increase in the toughness of the material.

In the presented set-up, α and β are determined by energy minimisation, which in turn determine $\tilde{f},\tilde{g}$. The functions f and g diverge for values of α and β that correspond to the locations of the isotropic defects. Since these defects have a size, the divergence of f and g has a natural cutoff. In fact, the isotropic defects are randomly distributed rather than forming an ordered array. An effective way of taking this into account is to take α and β to be random functions of the quadrupole positions – describing the random location of each quadrupole with respect to the isotropic defects structure. In this case, the slope that we calculated is also position dependent – that is adding a single quadrupole at some position may be very expensive energetically, while for another position it can reduce the energy. Accordingly, while some values of α and β encourage the formation of quadrupoles, other

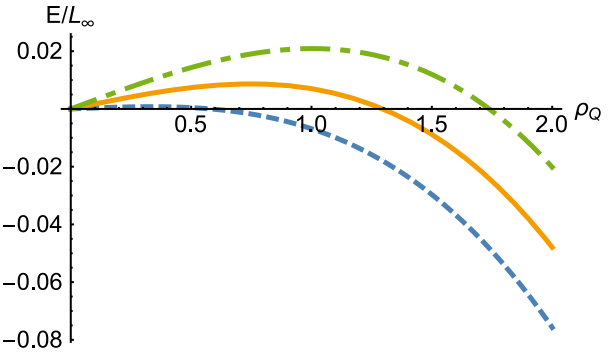

Figure 10. (colour online) Energy density as a function of quadrupole density. The yellow continuous line corresponds to $(\alpha, \beta) = (0.85, 0.15)$. The blue dashed line is for $(\alpha, \beta) = (0.15, 0.5)$. The green dashed dotted line is for $(\alpha, \beta) = (0.15, 0.15)$. The parameters used for this plot are: $P/lp^2 = -0.01, Q = 0.158$. The external shear strain is the yield strain corresponding to $P = 0$, $\gamma = Q/(16\pi a^2)$.

values suppress it. In Figure 10 we plot the energy density as a function of quadrupole density for different values of α and β.

In order to prevent the formation of a macroscopic shear band, it is enough to suppress the formation of quadrupoles at some region. This will prevent the formation of a system-spanning array of quadrupoles. The fact that the slope for the energy associated with the formation of quadrupoles become positive at some regions shows that a random distribution of isotropic defects prevent the formation of system-spanning array of quadrupoles.

We therefore predict that a random distribution of isotropic defects allow for the formation of *finite* linear arrays of quadrupoles, whose lengths are determined by the density and magnitudes of the isotropic defects, and by the magnitude of the external shear. For large enough, but finite, external shear the mean length of a linear array of quadrupoles will reach the system size and a system spanning shear-band will form.

It is now left to show that by increasing η the slope of the energy density vs. quadrupole density, increases. In Figure 11, we plot the energy density as a function of the quadrupole density for several values of η.

Finally, we want to find quantitatively how the toughness of the material is improved by increasing η. In Figure 12, we plot the percentage change of yield strain, as a function of η. We see that for small values of η the effect is linear in η. For these small values of η we can get an increase of 60% in yield strain. These results depend also on the core size of the isotropic defects. We chose (α, β) to be as close as possible to one isotropic defect. For smaller cutoffs, the increase in yield strain will be larger. In the discussion section, we will explain that for much larger values of η the effect reverses and finally disappears.

In summary, we showed that the presence of isotropic defects may encourage or discourage locally the formation of quadrupoles. Since a shear-band requires the formation of a system spanning array of quadrupoles, it is enough to focus on the neighbourhoods in which quadrupole formation is suppressed. The formation of a system spanning linear array of quadrupoles will always be frustrated in regions that are close to an isotropic defect that happen to increase the interaction energy. A random distribution of isotropic defects will result in regions for which the slope of the energy density becomes positive and large. For a dilute distribution of isotropic defects the slope of the energy density may

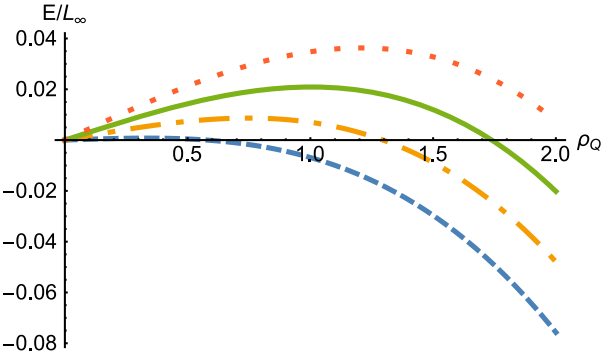

Figure 11. (colour online) Energy density as a function of quadrupoles density for several values of η, and for $(\alpha, \beta) = (0.15, 0.85)$. All parameters are fixed. The external shear corresponds to the yield strain for $\eta = 0$. Increasing $|\eta|$ result with a larger slope, hence there are regions for which the formation of quadrupoles is energetically unfavourable.

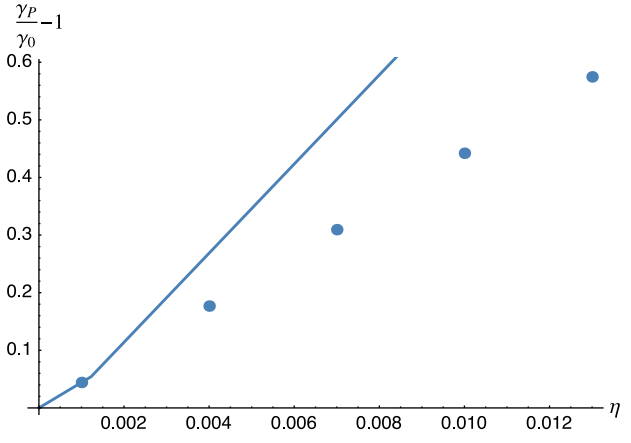

Figure 12. (colour online) The percentage change in yield strain at $\rho_q = 0$, for several values of $\eta = P/l_p^2$. For $\eta = 0$ there is no change in yield strain.

increase up to 60%, preventing the formation of system-spanning arrays of quadrupoles. The mechanism described here is independent of the sign of the charge of the isotropic defects. The upshot of this discussion is that we expect to find in such materials 'nano-shearband' whose lengths are determined by the isotropic defects distribution, and by the external shear γ.

4. Estimating the length of arrested shear bands

In this section, we examine the consequences of having a percentage c of microalloying particles in the amorphous material. Let us assume that each such particle organises a patch around it involving $n \sim O(10^2)$ other particles of the surrounding material. Then a fraction f of the material where

$$f = nc\,, \tag{36}$$

will consist of such patches. As at higher concentrations patches can overlap, the associated volume fraction of organised material ϕ will be

$$\phi = 1 - e^{-f} \,. \tag{37}$$

It is likely that the effect of the microalloying elements would be at its maximum when the patches begin to percolate and span the system. By 'percolation' here we assume the universality class of two-dimensional continuum percolation with circular inclusions. In this class the critical value for percolation is $\phi_c \approx 0.67$ and $f_c \approx 1.13$ [26]. This agrees with the order of magnitude of $c_c \approx 1\%$ which is a commonly quoted efficacious percentage for microalloying particles. For higher concentrations the effect of the microalloying particles can no longer be considered as 'defects'. Their surrounding start to become the whole material, and our discussion above stops being relevant.

Let us first consider $c \ll c_c$. In this regime the typical distance between microalloying particles and plastic quadrupoles is ξ,

$$\xi = c^{-1/2}\lambda \,, \tag{38}$$

where λ is the typical interatomic distance. In comparison, the radius of a single patch is about $a_{\rm iso} \approx \sqrt{n}\lambda \approx 10\lambda$. Thus at very low values of c, $\xi \gg a_{\rm iso}$.

At this point, consider such a density of $\ell = 0$ defects and a strained system that is attempting to create a shear band by aligning quadrupoles along a single line. With random distribution of the defects we expect a typical distance to the line of defects to be of the order of ξ. Taking into account the perturbation effect of the $\ell = 0$ defect on the shear banding instability discussed above, we can expect that no nano shear-band will form longer than a length of the order of ξ. With the numbers considered above we expect the nano shear-bands to have a length of the order of 150–500 Å. We note that this prediction can be put to direct experimental test by changing c and measuring the observed length of micro shear bands in the material.

With increasing the percentage c of microalloying particles, one expects that all the material parameters will change, including density, conductivities, the elastic moduli and the yield stress. Though an exact calculation of the dependence of all these material parameters on c is a complex problem, one can make a simple mean field estimate by applying the rule of mixtures to the particular material property of interest. For example, let us consider the shear modulus μ and its dependence on c in a block of material under uniaxial tension σ. We will need to specify the shear modulus of the background material in the absence of microalloying to be μ_m and the shear modulus of the $\ell = 0$ inclusions to be μ_i (naturally, depending on the material involved, $\mu_i > \mu_m$ or $\mu_i < \mu_m$). Also as the stress is homogenous we expect $\sigma_m = \sigma_i = \sigma$. As the total strain in the material is $\epsilon = \phi\epsilon_i + (1-\phi)\epsilon_m$ we find

$$\mu(c) = \frac{1}{(1-e^{-nc})/\mu_i + e^{-nc}/\mu_m}. \tag{39}$$

Similar arguments can be made for thermal and electrical conductivities. A particular simple case is the mass density $\rho = \phi\rho_i + (1-\rho)\rho_m$ or

$$\rho(c) = (1 - e^{-nc})\rho_i + e^{-nc}\rho_m. \tag{40}$$

Such mean-field arguments are valid for $c < c_c$ where disconnected clusters of inclusions can be expected to exist. The size of these patches diverge as $\sim (c_c - c)^{-\nu}$ and above the percolation transition macroscopic networks of patches can be expected to exist which will fundamentally change the material properties of the microalloyed sample.

5. Discussion

We have used the previously obtained understanding of the fundamental plastic instability that leads to the appearance of shear-bands in amorphous solids to shed light on why and to what extent the addition of a minute concentration of foreign atoms can defer this instability and improve the toughness of the material. The mechanism is simple; in the absence of microalloying elements the shear band is formed by a system spanning line of Eshelby-like quadrupolar displacement fields that combine together to form a shear-band. To form a displacement field that is a shear-band the quadrupoles must have a uniform and identical orientation. Isotropic defects interact with the incipient quadrupoles, forcing them to turn their orientation to minimise the interaction energy. This results in a perturbation of the perfect 'in phase' ordering of the quadrupoles that is necessary for the creation of the shear-band. This perturbation can be overcome by increasing the external shear strain whose effect is to reorganise the quadrupoles to be in phase. This is precisely the proposed explanation to the data shown in Figure 1.

The mechanism proposed offers also predictions on the non-spanning nano shear-bands that can be observed in the strained materials, and their dependence on the concentration of the microalloying elements. These predictions are easy to check experimentally and we hope that such measurements would be achieved soon.

Acknowledgement

M.M. is grateful to Prof. Raz Kupferman and to Prof. Eran Sharon for their support and useful discussions.

Disclosure statement

No potential conflict of interest was reported by the authors.

Funding

This work had been supported in part by and ERC 'ideas' grant STANPAS. M.M. was supported by the Israel-US Binational Foundation [grant number 2010129]; Israel Science Foundation [grant number 661/13].

References

[1] W. Buckel and R. Hilsch, *Einflußder Kondensation bei tiefen Temperaturen auf den elektrischen Widerstand und die Supraleitung für verschiedene Metalle* [Influence of low-temperature condensation on the electrical resistance and superconductivity of various metals], Z. Phys. 138 (1954), pp. 109–120.

[2] W. Klement, R.H. Willens, and P.O.L. Duwez, Non-crystalline structure in solidified gold–silicon alloys. 187 (1960), pp. 869–870.
[3] A. Inoue, *Stabilization of metallic supercooled liquid and bulk amorphous alloys*, Acta Mater. 48 (2000), pp. 279–306.
[4] A. Peker and W.L. Johnson, *A highly processable metallic glass: Zr41. 2Ti13. 8Cu12. 5Ni10. 0Be22. 5*, Appl. Phys. Lett. 63 (1993), pp. 2342–2344.
[5] Q. Wang, C.T. Liu, Y. Yang, J.B. Liu, Y.D. Dong, and J. Lu, *The atomic-scale mechanism for the enhanced glass-forming-ability of a Cu–Zr based bulk metallic glass with minor element additions*, Sci. Rep. 4 (2014); see e.g. Ref. 5 and US Patent 2015/0159242 A1, June 11, 2015.
[6] J.H. Na, M.D. Demetriou, M. Floyd, A. Hoff, G. Garrett, and W.L. Johnson, *Compositional landscape for glass formation in metal alloys*, Proc. Nat. Acad. Sci. 111 (2014), pp. 9031–9036.
[7] S.M. Chathoth, B. Damaschke, T. Unruh, and K. Samwer, *Influence of structural changes on diffusion in liquid germanium*, Appl. Phys. Lett. 94 (2009), p. 221906.
[8] H.W. Sheng, W.K. Luo, F.M. Alamgir, J.M. Bai, and E. Ma, *Atomic packing and short-to-medium-range order in metallic glasses*, Nature 439 (2006), pp. 419–425.
[9] J. Krausser, K. Samwer, and A. Zaccone, *Interatomic repulsion softness directly controls the fragility of supercooled metallic melts*, Proc. Nat. Acad. Sci. 112 (2015), pp. 13762–13767.
[10] D. Kivelson, S.A. Kivelson, X. Zhao, Z. Nussinov, and G. Tarjus, *A thermodynamic theory of supercooled liquids*, Phys. A: Stat. Mech. Appl. 219 (1995), pp. 27–38.
[11] P.G. De Gennes, *A simple picture for structural glasses*, C.R. Phys. 3 (2002), pp. 1263–1268.
[12] N. Mattern, P. Jvri, I. Kaban, S. Gruner, A. Elsner, V. Kokotin, H. Franz, B. Beuneu, and J. Eckert, *Short-range order of Cu–Zr metallic glasses*, J. Alloys Compd. 485 (2009), pp. 163–169.
[13] K. Saksl, H. Franz, P. Jvri, K. Klementiev, E. Welter, A. Ehnes, J. Saida, A. Inoue, and J.Z. Jiang, *Evidence of icosahedral short-range order in Zr70Cu30 and Zr70Cu29Pd1 metallic glasses*, Appl. Phys. Lett. 83 (2003), pp. 3924–3926.
[14] Ch.E Lekka, A. Ibenskas, A.R. Yavari, and G.A. Evangelakis, *Tensile deformation accommodation in microscopic metallic glasses via subnanocluster reconstructions*, Appl. Phys. Lett. 91 (2007), p. 4103.
[15] S.-C. Lee, C.-M. Lee, J.-C. Lee, H.-J. Kim, Y. Shibutani, E. Fleury, and M.L. Falk, *Structural disordering process of an amorphous alloy driven by the elastostatic compression at room temperature*, Appl. Phys. Lett. 92 (2008), p. 151906.
[16] F.C. Frank and J.S. Kasper, *Complex alloy structures regarded as sphere packings. I. Definitions and basic principles*, Acta Crystallogr. 11 (1958), pp. 184–190.
[17] J.D. Eshelby, *The determination of the elastic field of an ellipsoidal inclusion, and related problems. Proc. R. Soc. London A: Math. Phys*, Eng. Sci. 241 (1957), pp. 376–396.
[18] A.S. Argon and H.Y. Kuo, *Plastic flow in a disordered bubble raft (an analog of a metallic glass)*, Mat. Sci. Eng. 39 (1979), pp. 101–109; A.S. Argon, *Plastic deformation in metallic glasses*, Acta Metall. 27 (1979), pp. 47–58; A.S. Argon and L.T. Shi, *Analysis of plastic flow in an amorphous soap bubble raft by the use of an inter-bubble potential*, Philos. Mag. 46 (1982), pp. 275–294.
[19] R. Dasgupta, S. Karmakar, and I. Procaccia, *Universality of the plastic instability in strained amorphous solids*, Phys. Rev. Lett. 108 (2012), pp. 075701-1–075701-4.
[20] R. Dasgupta, H.G.E. Hentschel, and I. Procaccia, *Yield strain in shear banding amorphous solids*, Phys. Rev. E 87 (2013), pp. 022810-1–022810-14.
[21] R. Dasgupta, H.G.E. Hentschel, and I. Procaccia, *Microscopic mechanism of shear bands in amorphous solids*, Phys. Rev. Lett. 109 (2012), pp. 255502-1–255502-4.
[22] J. Ashwin, O. Gendelman, I. Procaccia, and C. Shor, *The yield-strain and shear-band direction in amorphous solids under general loading*, Phys. Rev. E. 88 (2013), pp. 022310-1–022310-12.
[23] M. Moshe, I. Levin, H. Aharoni, R. Kupferman, and E. Sharon, *Geometry and mechanics of two-dimensional defects in amorphous materials*, Proc. Nat. Acad. Sci. 112 (2015), pp. 10873–10878.
[24] M. Moshe, E. Sharon, and R. Kupferman, *Elastic interactions between two-dimensional geometric defects*, Phys. Rev. E 92 (2015), pp. 062403-1–062403-8.

[25] N. Zheng, R.T. Qu, S. Pauly, M. Calin, T. Gemming, Z.F. Zhang, and J. Eckert, *Design of ductile bulk metallic glasses by adding "soft" atoms*, Appl. Phys. Lett. 100 (2012), p. 141901.
[26] S.B. Lee and S. Torquato, *Monte Carlo study of correlated continuum percolation: universality and percolation thresholds*, Phys. Rev. A 41 (1990), pp. 5338–5344.
[27] L. Liu et al., *Improvements in the plasticity and biocompatibility of Zr–Cu–Ni–Al bulk metallic glass by the microalloying of Nb*, Mater. Sci. Eng. A. 449 (2007), pp. 193–197.

Appendix 1. The numerical protocol

In our AQS numerical simulations we use a 50–50 binary Lennard-Jones mixture to simulate the shear localisation discussed in this work. The potential energy for a pair of particles labeled i and j has the form

$$\begin{aligned} U_{ij}(r_{ij}) &= 4\epsilon_{ij}\Big[\Big(\frac{\sigma_{ij}}{r_{ij}}\Big)^{12} - \Big(\frac{\sigma_{ij}}{r_{ij}}\Big)^{6} + A_0 \\ &\quad + A_1\Big(\frac{r_{ij}}{\sigma_{ij}}\Big) + A_2\Big(\frac{r_{ij}}{\sigma_{ij}}\Big)^2\Big], \end{aligned} \tag{A1}$$

where the parameters A_0, A_1 and A_2 are added to smooth the potential at a scaled cut-off of $r/\sigma = 2.5$ (up to the second derivative). The parameters σ_{AA}, σ_{BB} and σ_{AB} were chosen to be $2\sin(\pi/10)$, $2\sin(\pi/5)$ and 1 respectively and $\epsilon_{AA} = \epsilon_{BB} = 0.5, \epsilon_{AB} = 1$. The particle masses were taken to be equal. The samples were prepared using high-temperature equilibration followed by a quench to zero temperature ($T = 0.001$). For shearing, the usual athermal-quasistatic shear protocol was followed where each step comprises of an affine shift followed by an non-affine displacement using conjugate gradient minimisation. Explicitly, in two dimensions the affine state is achieved by moving the coordinates of every particle i according to

$$\begin{aligned} x_i &\to x_i + \delta\gamma y_i \\ y_i &\to y_i. \end{aligned} \tag{A2}$$

In an amorphous solid this affine step results in throwing all the forces on the particles out of balance. Accordingly, to regain mechanical equilibrium, one needs to execute a non-affine step, which is achieved by gradient energy minimisation. Once executed, the next step of straining is done. Note that in such quasi-static protocols there strain rate is zero.

The simulations were conducted in two dimensions (2d) and employed Lees-Edwards periodic boundary conditions. Samples were generated with quench rates ranging from 3.2×10^{-6} to 3.2×10^{-2} (in LJ units), and were strained to greater than 100%. Simulations were performed on system-sizes ranging from 5000 to 20,000 particles with a fixed density of $\rho = 0.976$ (in LJ units). The simulations reported in the paper have 10,000 particles and a quench-rate of 6.4×10^{-6} (in LJ units).